# High-temperature environments of human evolution in East Africa based on bond ordering in paleosol carbonates

Benjamin H. Passey[a,1,2], Naomi E. Levin[a,1], Thure E. Cerling[b], Francis H. Brown[b], and John M. Eiler[a]

[a]Division of Geological and Planetary Sciences, California Institute of Technology, Pasadena, CA 91125; and [b]Department of Geology and Geophysics, University of Utah, Salt Lake City, UT 84112

Edited* by Karl K. Turekian, Yale University, New Haven, CT, and approved May 14, 2010 (received for review February 12, 2010)

**Many important hominid-bearing fossil localities in East Africa are in regions that are extremely hot and dry. Although humans are well adapted to such conditions, it has been inferred that East African environments were cooler or more wooded during the Pliocene and Pleistocene when this region was a central stage of human evolution. Here we show that the Turkana Basin, Kenya—today one of the hottest places on Earth—has been continually hot during the past 4 million years. The distribution of $^{13}C$-$^{18}O$ bonds in paleosol carbonates indicates that soil temperatures during periods of carbonate formation were typically above 30 °C and often in excess of 35 °C. Similar soil temperatures are observed today in the Turkana Basin and reflect high air temperatures combined with solar heating of the soil surface. These results are specific to periods of soil carbonate formation, and we suggest that such periods composed a large fraction of integrated time in the Turkana Basin. If correct, this interpretation has implications for human thermophysiology and implies a long-standing human association with marginal environments.**

continental paleoclimate | clumped isotopes | soil temperature | hominid | bipedal locomotion

The environmental context of human evolution in eastern Africa is widely believed to feature increased seasonal aridity and related habitat change from forested to more open, savanna-type ecosystems, in part owing to differential surface uplift associated with the creation of the East African Rift System (1). Fossil records of mollusks (2), mammals (3, 4), plants (5, 6), and carbon isotopes (indicative of tropical $C_4$ grasses) (7, 8) generally suggest that habitats became less wooded and more open during the Pliocene and Pleistocene. Less is known of the temperature history of Africa—or the continental tropics in general—during this time period. A land-based, high-resolution temperature record from eastern Africa, constructed using empirical paleotemperature proxies based on fossil pollen assemblages (6), suggests that late Pliocene temperatures were cooler than present. However, it is also commonly inferred that Africa was warmer in the past (3, 4, 9), on the basis of analogy with the record of cooling and increased glaciation in the Northern Hemisphere during the past 3 million years. Although there is ample evidence of environmental change in the tropics, including changes in the frequency spectrum and amount of dust transported from Africa to nearby seas (10), it is difficult to relate these records to temperature.

We address the temperature history of the Turkana Basin in northern Kenya (Fig. 1) by applying the carbonate clumped-isotope thermometer (11) to fossil soil (paleosol) carbonates. The Turkana Basin, whose present mean annual temperature of 29.2 °C places the region in the hottest ~1% of continental land areas (12) (Fig. 2), is a key locale in human evolution with a rich fossil record of hominins and associated fauna (13). Our geochemical approach is based on the temperature-dependent formation of $^{13}C$-$^{18}O$ bonds in carbonate minerals. Unlike the widely used $\delta^{18}O$-in-carbonate paleothermometer, the clumped isotope approach requires no assumptions about the $\delta^{18}O$ of the water in which the mineral formed: A single laboratory measurement provides the formation temperature, $\delta^{13}C$, and $\delta^{18}O$ of carbonate and allows for calculation of $\delta^{18}O$ of the parent water. This method conforms to a single calibration for a variety of carbonates, including inorganic calcite, corals, aragonitic fish otoliths, foraminifera, coccoliths, and mollusk and brachiopod shells (14), whereas kinetic effects and departure from the inorganic calibration line have been described in speleothems (15).

Past studies have not demonstrated conclusively whether clumped isotope temperatures of modern soil carbonates record modern ground temperatures, so this study includes an examination of recent soil carbonates from Kenya, Ethiopia, China, and the United States to investigate appropriateness of this proxy to the materials and locations of interest to us. Analysis of carbonatites and marbles indicates that solid-state $^{13}C$-$^{18}O$ reordering is negligible over geological timescales at temperatures cooler than ~250 °C (16). Preservation of Earth-surface temperatures in soil carbonates as old as 25 Ma and buried to depths of ~5 km (with associated burial temperatures of ~150 °C) demonstrates that this system can be refractory with respect to near-surface postdepositional alteration (17), although this issue must still be considered for our study, as near-surface processes such as dissolution and reprecipitation will reset the clumped isotope signal.

## Results and Discussion

**Recent Soil Carbonates.** Climate data for recent soil carbonate localities are given in Table S1, and the temperatures of recent soil carbonates determined using the carbonate clumped isotope thermometer are shown in Fig. 3 and summarized in Table S2. For recent soil carbonates from Kenya and Ethiopia (tropical regions with little annual variability in temperature), we observe a close correspondence between soil temperatures inferred from the clumped isotope thermometer and mean annual air temperatures. For the higher latitude samples (California and China), clumped isotope temperatures are more similar to summer air temperatures, suggesting a seasonal bias in soil carbonate formation, possibly combined with an influence of solar heating in cases where the carbonates formed before or after warm-season air temperature maxima. Such seasonal bias in soil carbonate precipitation has been suggested on the basis of independent lines of evidence (18), and it appears that this will be an important

Author contributions: B.H.P., N.E.L., T.E.C., F.H.B., and J.M.E. designed research; B.H.P., N.E.L., T.E.C., F.H.B., and J.M.E. performed research; B.H.P., N.E.L., T.E.C., F.H.B., and J.M.E. analyzed data; and B.H.P. wrote the paper.

The authors declare no conflict of interest.

*This Direct Submission article had a prearranged editor.

[1]Present address: Department of Earth and Planetary Sciences, Johns Hopkins University, 301 Olin Hall, 3400 North Charles Street, Baltimore, MD 21218.

[2]To whom correspondence should be addressed. E-mail: bhpassey@jhu.edu.

This article contains supporting information online at www.pnas.org/lookup/suppl/doi:10.1073/pnas.1001824107/-/DCSupplemental.

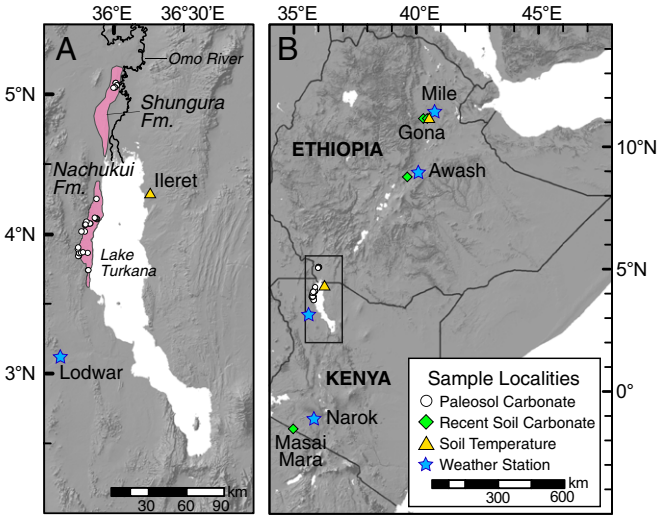


**Fig. 1.** Map of the study area in East Africa. (*A*) Detail map of the Turkana Basin showing sample locations for fossil paleosol carbonates (white circles). (*B*) Map of eastern Africa showing sample locations for recent soil carbonates (green diamonds), climate stations (blue stars), and locations of soil temperature measurements (orange triangles). Background images are shaded relief digital elevation models.

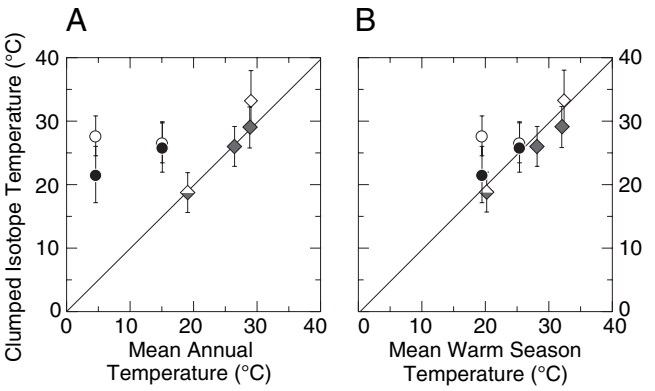


**Fig. 3.** (*A* and *B*) Clumped isotope temperatures of soil carbonates collected from recent soils from low latitudes (<12° absolute latitude, diamonds) and intermediate latitudes (34°N and 42°N, circles). Open, solid, and mixed symbols represent soil carbonates collected from <50 cm, ≥50 cm, or undocumented depth below the present soil surface. Error bars are SDs for soils with multiple depth-resolved samples or the average SD of replicate analysis for soils with single samples. (*B*) Mean warm season temperature is taken as the average temperature of the three warmest consecutive months of the year. The data are reported in Table S2.

consideration when applying the clumped isotope approach to soil carbonates formed in temperate climates. This seasonal bias should be less important in low latitudes where seasonality in temperature is minimal. For instance, the annual range in average monthly temperature near our study area at Lodwar, Kenya (Fig. 1) is 1.8 °C, and the average annual range for 14 meteorological stations across Kenya is 3.1 °C (19). However, seasonal variability in soil temperature may be larger owing to changes in soil moisture and insolation, as illustrated by soil temperature measurements near Lake Turkana (Fig. S1 and Table S3).

Finally, we cannot rule out the possibility that apparent clumped isotope temperatures are influenced by kinetic effects during carbonate precipitation. However, the deep soil environment (~ >50 cm) is buffered from rapid changes in temperature, moisture, and $pCO_2$, and this buffer might reduce opportunities for calcite precipitation under nonequilibrium conditions. We observe some tendency for shallow soil carbonates (<45 cm) to record higher apparent "clumped isotope" temperatures than deep soil carbonates in recent soils (Fig. 3 and Table S2), although this pattern is poorly defined and is not observed in all samples.

**Paleosol Carbonates.** Isotopic analysis was restricted to carbonates collected from depths of ≥50 cm below the preserved upper surface of each paleosol horizon. The mass-47 enrichments of $CO_2$ extracted from paleosol carbonates (expressed as values of $\Delta_{47}$, *Methods*) range between 0.58 and 0.63‰, indicating that soil temperatures during periods of carbonate formation were between 41 and 28 °C (Fig. 4 and Table S4). There are no clearly resolvable temporal trends in these data, and the mean temperature recorded by paleosol carbonates is 33.2 °C, or 4.0 °C higher than present-day mean annual temperature (MAT), and comparable to modern soil temperatures (Fig. S1 and Table S3). Because soil temperature at >50 cm depth represents a time-

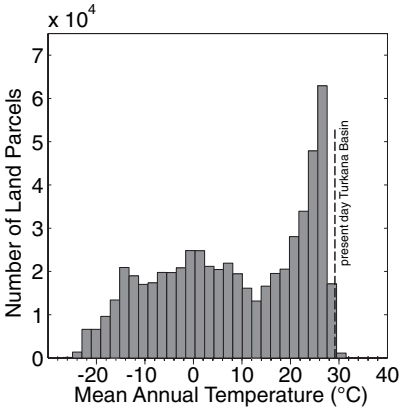


**Fig. 2.** Global distribution of mean annual temperatures. The histogram is a compilation of mean annual temperatures of all land parcels exclusive of Antarctica (10′ x 10′ grid) in the WorldClim global climatology (12). The Turkana Basin presently has a mean annual temperature of ~29 °C, ranking it among the hottest places on Earth.

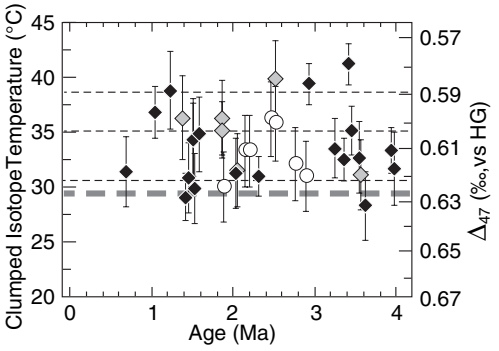


**Fig. 4.** Clumped isotope temperatures of paleosol carbonates from the Nachukui and Shungura formations (solid diamonds and open circles, respectively), Turkana Basin, Kenya, and Ethiopia. Results from nonpedogenic authigenic carbonates from the Nachukui Formation are shown by shaded diamonds. Error bars are SEs, calculated as detailed in *SI Text*. The thick dashed line represents the present-day mean annual air temperature in the study area (meteorological data from Lodwar, Kenya). The thin dashed lines represent the minimum, mean, and maximum soil temperatures observed at 50 cm depth over a 9-mo interval in the study area (Ileret, Kenya; Fig. S1 and Table S3). The data are reported in Table S4.

integrated average of daytime and nighttime soil surface temperatures, these temperatures indicate that daytime surface soil temperatures were well in excess of 28–41 °C.

There are no clear relationships between soil temperature and orbital eccentricity, obliquity, precession, or solar insolation, although such analysis for the higher-frequency signals (precession and solar insolation) is limited by the ~40- to 100-ka age uncertainty of each sampling horizon (*SI Text*). There are no correlations between soil carbonate $\Delta_{47}$ and $\delta^{13}C$, $\delta^{18}O$, or calculated soil water $\delta^{18}O$. Additionally, there is no correlation between $\Delta_{47}$ and burial depth (Fig. 5) such as would be indicative of $^{13}C$-$^{18}O$ bond reordering at elevated temperatures during burial.

**Climatic Significance of Ground Temperature.** To interpret the isotopic paleotemperature record, we further consider how soil temperatures relate to air temperatures. To first order, soil temperature at ~50 cm depth approximates mean annual air temperature in tropical regions that exhibit little seasonal variation in air temperature, or seasonally averaged air temperature in regions with significant seasonality of temperature (20). Superimposed on the air temperature effect, solar heating of the soil surface acts to further elevate soil temperatures. This solar-heating effect is important to the interpretation of our data because it is the soil surface temperature, rather than air temperature, that is the dominant boundary condition controlling soil temperature at depth (20). This phenomenon is illustrated by measurements of soil temperature in immediately adjacent shaded and sunny locations (21, 22) and by contrasting temperatures of primary vs. disturbed tropical rainforest soils (Fig. S2). We logged soil temperatures at several sites relevant to this study (Table S3 and Fig. S1), including a 9-mo record at Ileret, Turkana Basin, Kenya. The average 50-cm-depth soil temperature at Ileret was 35 °C, or 4 °C higher than average air temperature measured in the same location. Daytime air temperatures were typically in the range of 35–40 °C, and heat flow calculations (23) suggest that daytime soil-surface temperatures were commonly in excess of 50 °C.

**Plio-Pleistocene Paleoenvironments in the Turkana Basin.** The similar-to-present soil temperatures indicated for the paleosol carbonates are inconsistent with cooler and more vegetated (shaded) conditions compared with the present day. And, because the present environment is already arid, sunny, and sparsely vegetated, there is little potential for additional solar heating. Thus, the Plio-Pleistocene environments recorded by clumped isotopes in paleosol carbonates were either similar to present environments or more vegetated but also warmer.

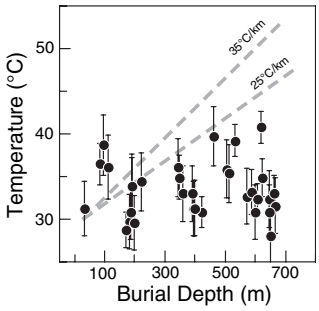


**Fig. 5.** Carbonate clumped isotope paleotemperatures (circles) and modeled maximum burial temperatures (dashed lines) plotted as a function of burial depth (Table S4). The burial temperatures are modeled for 35 °C/km and 25 °C/km geothermal gradients. There is no clear evidence of $^{13}C$-$^{18}O$ reordering in the paleosol carbonates resulting from diagenetic processes at depth (for example, dissolution/recrystalization, pressure solution, or other mechanisms of crystal coarsening).

As a limiting case of a "warmer and more vegetated" scenario, if the Turkana Basin was humid enough to be occupied by closed forest during the Pliocene and Pleistocene, soil temperatures would have been similar to air temperatures (because the forest canopy would make radiative heating negligible), and average air temperatures of ~33 °C would be required to explain our carbonate clumped isotope thermometry results. To place this temperature into context, today <1% of all tropical landmass (30°N to 30°S) has a mean annual temperature >30 °C, and of that receiving enough precipitation to support rainforest (here taken as >1,500 mm annually), <1% has a mean annual temperature >28 °C (12). Excluding gallery forest, we know of no forested site with MAT warmer than 30 °C.

Some previous studies have suggested that rainforest habitat existed in the Turkana Basin as recently as the late Pliocene, on the basis of occurrences of fossil animals (4) and plants (5) with closed-forest affinities. However, there is abundant coexisting evidence of drier habitats in the Turkana Basin. For example, soil carbonates, which are uncommon in regions receiving >1,000 mm of rainfall per annum (24), are common throughout Pliocene-aged sediments in the Turkana Basin, including the Nachukui and Shungura Formations examined here. Fossil ungulate taxa specialized for grazing are common in the Turkana Basin fossil record, and carbon isotope analyses of their tooth enamel, and also paleosol carbonates (Table S4), confirm that $C_4$ grasses were an important part of these ecosystems (25). The coexisting evidence for humid and dry habitats suggests that these habitats were juxtaposed in space, in time, or both. A probable explanation is that gallery forest existed alongside the ancient Omo River—as it does today—and that it fluctuated in extent as climate cycled between humid and arid phases.

**Climate Variability and Periods of Soil Carbonate Formation.** Orbital-scale climate variability is well documented in this low-latitude setting (10) and has been cited as an important factor in shaping the course of human evolution (9). An intrinsic feature of our soil temperature proxy is that it records soil temperature during times of carbonate mineralization. Therefore it is important to examine whether these soil carbonates formed under a wide range of prevailing climates, or under a restricted range of prevailing climates. Paleosol carbonates are common in the Pliocene and Pleistocene strata of the Turkana Basin, and because the depositional regime was primarily fluvial, soils would have existed at all times and places except in the vicinity of active channels. Therefore, if soil carbonates formed only under very specific conditions, we would expect paleosol carbonates to be present in only a small fraction of paleosols. Although there are not yet quantitative data on the fraction of paleosols with soil carbonates, it is our experience that most of the paleosols host paleosol carbonates. In addition, the $\delta^{13}C$, $\delta^{18}O$, and $\Delta_{47}$ values of the paleosols are variable on short (<100 ka) timescales, indicating that soil carbonates formed under a variety of prevailing vegetation types, hydrological conditions, and temperatures. Although the relatively low sampling resolution and sample age uncertainties (~40–100 ka) (26, 27) do not permit correlation to precessional cycles, the resolution and dating are sufficient to show that soil carbonates developed under a range of eccentricity configurations. Finally, the $\delta^{13}C$ and $\delta^{18}O$ values show clear secular trends indicating a progressive increase through time of $C_4$ grasses ($\delta^{13}C$) and a major change in regional circulation, humidity, or basin hydrology ($\delta^{18}O$) after 2 Ma (ref. 7 and Table S4). These lines of evidence collectively suggest that soil carbonates formed under a variety of prevailing conditions. Because soils and soil carbonates develop over long timescales ($10^2$–$10^5$ y) (28) and are common throughout strata in the Turkana Basin (8), they must record a suite of frequently recurring environmental conditions.

**Implications for Human Thermophysiology.** This temperature record is relevant to the evolutionary origin or maintenance of a unique suite of adaptations that permit humans to remain active under high ambient heat loads. For example, upright posture in hot, open environments confers thermophysiological advantages to bipedal hominins owing to reduced interception of direct solar radiation and to displacement of the body away from the near-surface environment, which may be excessively hot due to solar heating (29). Derived human traits such as very little body hair, high sweating capacity, and high surface area to volume ratio are also advantageous for daytime activity in hot, arid climates (30), and temperature is a central variable in hypotheses of behaviors such as long-distance scavenging and persistence hunting (31). However, the thermoregulatory advantages of these adaptations arise primarily under very hot, sunny conditions (29, 32, 33). Our results suggest that such conditions were relevant to human ecology in the Turkana Basin, either directly within or at the spatial or temporal margins of human-preferred habitats.

## Conclusions

The data presented here demonstrate that clumped isotope temperatures of recent soil carbonates are related to climate and environment. The effects of solar heating or, conversely, shade are important to the interpretation of clumped isotope temperature data, and seasonality of carbonate precipitation is an important factor in temperate climates, where soil carbonates appear to record warm season temperatures. This seasonal bias is less apparent in tropical latitudes, where seasonality in air temperature is typically less than a few degrees.

The temperatures of carbonate formation inferred for Pliocene and Pleistocene paleosol carbonates from the Turkana Basin are similar to present-day soil temperatures. Because both air temperature and solar radiation control soil temperature at depth, these data are inconsistent with the hypothesis that past environments were cooler and more vegetated than today (at least, during periods of soil carbonate formation) and suggest that past environments were similar to, or warmer and more vegetated than, present-day environments. Thus, for example, modern Kenyan savanna environments like Nakuru, Maasai Mara, or Amboseli are not particularly good analogs for Turkana Basin paleoenvironments, because their temperatures are far lower (MAT = 17, 19, and 25 °C, respectively) than those inferred here (~ ≥30 °C). If past environments were more vegetated, a more suitable analog may be the grassland–bush–gallery forest environment typical of the lower Omo River valley north of Lake Turkana.

It is likely that numerous independent factors were involved in the evolutionary origin and maintenance of traits such as bipedal locomotion, slender body form, reduction of functional body hair, and high sweating capacity. Whereas our data are silent on the *importance* of ambient temperature in shaping human evolution, they comprise a necessary prerequisite for beginning to evaluate temperature-related hypotheses.

## Methods

Carbonate nodules were collected from paleosols that are interbedded with fluvial, alluvial, and lacustrine sediments of the Nachukui and Shungura Formations in northern Kenya. These were collected ≥50 cm below the preserved upper surfaces of soil horizons. A small number of nonpedogenic carbonates were sampled, including crack-fill and ledge-type cements. Soil carbonates collected from recent soils included nodular, pendant (clast-coating), and crack- and ledge-type morphologies. Subsamples were examined and fine-grained (micritic) fractions were selected for isotopic analysis. The micritic texture of the fossil soil carbonates is similar to that observed for recent soil carbonates, suggesting that they were not recrystallized during burial. Isotopologue measurements were carried out using an automated carbonate device (Fig. S3) coupled to a Thermo MAT 253 mass spectrometer at the California Institute of Technology. Briefly, samples were reacted at 90 °C in 100% $H_3PO_4$, and the $CO_2$ product was purified by passage through multiple cryogenic traps, including a Porapak-Q gas chromatograph (GC) column held at −20 °C. Mass 44-normalized ion ratios of all stable $CO_2$ isotopologue masses (45/44, 46/44, 47/44, 48/44, and 49/44) were measured, and the parameter $\Delta_{47}$ was calculated as

$$\Delta_{47} = \left[\left(\frac{R^{47}}{R^{47*}} - 1\right) - \left(\frac{R^{46}}{R^{46*}} - 1\right) - \left(\frac{R^{45}}{R^{45*}} - 1\right)\right] \times 1{,}000,$$

where

$$R^i = \frac{\text{mass } i}{\text{mass } 44}.$$

The parameter $R^{i*}$ is analogous to $R^i$, but corresponds to ratios for the same sample with a stochastic distribution of isotopologues. All data were normalized to $CO_2$ gases heated to 1,000 °C to achieve stochastic distribution of isotopologues. A correction of +0.081‰ was applied to all $\Delta_{47}$ data to account for the difference in phosphoric acid reaction temperature between this study (90 °C) and that of the original temperature calibration (25 °C; ref. 11) (Table S5). Finally, small (typically $<<\pm 0.02$‰) corrections were applied based on deviations from accepted values of in-house standards analyzed concurrently with the samples (Fig. S4; Dataset S1). Detailed methods are provided in *SI Text*.

**ACKNOWLEDGMENTS.** We thank A. Sessions, W. Brand, J. Eronen, and C. Baumgartner for technical advice; C. Remien for help with temperature measurements; D. Bramble, J. Quade, and S. Simpson for commenting on earlier versions of the manuscript; and the editor and reviewers for insightful comments and suggestions. We thank the Dreyfus Foundation and the National Science Foundation for supporting this research.

1. Sepulchre P, et al. (2006) Tectonic uplift and Eastern Africa aridification. *Science* 313: 1419–1423.
2. Williamson PG (1985) Evidence for an early Plio-Pleistocene rainforest expansion in East Africa. *Nature* 315:487–489.
3. Bobe R, Behrensmeyer AK, Chapman RE (2002) Faunal change, environmental variability and late Pliocene hominin evolution. *J Hum Evol* 42:475–497.
4. Fernández MH, Vrba ES (2006) Plio-Pleistocene climatic change in the Turkana Basin (East Africa): Evidence from large mammal faunas. *J Hum Evol* 50:595–626.
5. Bonnefille R (1995) *A Reassessment of the Plio-Pleistocene Pollen Record of East Africa* (Yale Univ Press, New Haven, CT).
6. Bonnefille R, Potts R, Chalié F, Jolly D, Peyron O (2004) High-resolution vegetation and climate change associated with Pliocene *Australopithecus afarensis*. *Proc Natl Acad Sci USA* 101:12125–12129.
7. Cerling TE, Bowman JR, O'Neil JR (1988) An isotopic study of a fluvial-lacustrine sequence: The Plio-Pleistocene koobi fora sequence, East Africa. *Palaeogeogr Palaeoclimatol Palaeoecol* 63:335–356.
8. Wynn JG (2004) Influence of Plio-Pleistocene aridification on human evolution: Evidence from paleosols of the Turkana Basin, Kenya. *Am J Phys Anthropol* 123: 106–118.
9. Potts R (2007) Environmental hypotheses of Pliocene human evolution. *Hominin Environments in the East African Pliocene. Assesment of the Faunal Evidence, Vertebrate Paleobiology and Paleoanthropology Series*, eds Bobé R, Alemseged Z, Behrensmeyer AK (Springer, Dordecht, the Netherlands).
10. deMenocal PB (2004) African climate change and faunal evolution during the Pliocene–Pleistocene. *Earth Planet Sci Lett* 220:3–24.
11. Ghosh P, et al. (2006) $^{13}C$-$^{18}O$ bonds in carbonate minerals: A new kind of paleothermometer. *Geochim Cosmochim Acta* 70:1439–1456.
12. Hijmans RJ, et al. (2000) Very high resolution interpolated climate surfaces for global land areas. *Int J Climatol* 25:1965–1978.
13. Bobe R, Leakey MG (2009) Ecology of Plio-Pleistocene mammals in the Omo-Turkana Basin and the emergence of Homo. *The First Humans—Origin and Early Evolution of the Genus Homo*, eds Grine FE, Fleagle JG, Leakey RG (Springer, Berlin), pp 173–184.
14. Eiler JM (2007) "Clumped-isotope" geochemistry—The study of naturally-occurring, multiply-substituted isotopologues. *Earth Planet Sci Lett* 262:309–327.
15. Affek HP, Bar-Matthews M, Ayalon A, Matthews A, Eiler JM (2008) Glacial/interglacial temperature variations in Soreq cave speleothems as recorded by 'clumped isotope' thermometry. *Geochim Cosmochim Acta* 72:5351–5360.
16. Dennis KJ, Schrag DP (2010) Clumped isotope thermometry of carbonatites as an indicator of diagenetic alteration. *Geochim Cosmochim Acta*, 10.1016/j.gca.2010.04.005.
17. Eiler J, Garizone C, Ghosh P (2006) Response to comment on "Rapid uplift of the Altiplano revealed through $^{13}C$-$^{18}O$ bonds in paleosol carbonates". *Science* 314:760c.
18. Breeker DO, Sharp ZD, McFadden LD (2009) Seasonal bias in the formation and stable isotopic composition of pedogenic carbonate in modern soils from central New Mexico, USA. *Geol Soc Am Bull* 121:630–640.

19. East African Meteorological Department (1975) *Climatological Statistics for East Africa* (East African Meteorological Department, Nairobi, Kenya).
20. Geiger R, Aron RH, Todhunter P (2009) *The Climate Near the Ground* (Rowman & Littlefield, Lanham, MD) 7th Ed.
21. Tang JW, Baldocchi DD, Xu LK (2005) Tree photosynthesis modulates soil respiration on a diurnal time scale. *Glob Change Biol* 11:1298–1304.
22. Kos M, Poschlod P (2007) Seeds use temperature cues to ensure germination under nurse-plant shade in xeric Kalahari savannah. *Ann Bot (Lond)* 99:667–675.
23. Jury WA, Horton R (2004) *Soil Physics* (John Wiley & Sons, Hoboken, NJ), 6th Ed, p 370.
24. Royer DL (1999) Depth to pedogenic carbonate horizon as a paleoprecipitation indicator? *Geology* 27:1123–1126.
25. Cerling TE, Harris JM, Leakey MG (2003) *Stable Isotope Ecology of the Nawata and Apak Formations at Lothagam, Turkana Basin, Kenya* (Columbia Univ Press, New York).
26. McDougall I, Brown FH (2006) Precise 40Ar/39Ar geochronology for the upper Koobi Fora Formation, Turkana Basin, northern Kenya. *J Geol Soc London* 163:205–220.
27. McDougall I, Brown FH (2008) Geochronology of the pre-KBS Tuff sequence, Omo Group, Turkana Basin. *J Geol Soc London* 165:549–562.
28. Machette MN (1985) *Calcic Soils in the Southwestern United States* (Geological Society of America, Boulder, CO), pp 1–22.
29. Wheeler PE (1991) The thermoregulatory advantages of hominid bipedalism in open equatorial environments: The contribution of increased convective heat loss and cutaneous evaporative cooling. *J Hum Evol* 21:107–115.
30. Ruff CB (1993) Climatic adaptation and hominid evolution: The thermoregulatory imperative. *Evol Anthropol* 2:53–60.
31. Bramble DM, Lieberman DE (2004) Endurance running and the evolution of *Homo*. *Nature* 432:345–352.
32. Wheeler PE (1993) The influence of stature and body form on hominid energy and water budgets; a comparison of Australopithecus and early Homo physiques. *J Hum Evol* 24:13–28.
33. Wheeler PE (1992) The influence of the loss of functional body hair on the water budgets of early hominids. *J Hum Evol* 23:349–388.

# Supporting Information

## Passey et al. 10.1073/pnas.1001824107

### SI Text

**Soil Temperature Measurements.** Soil temperatures were logged at 20-min intervals over 9 mo at Ileret, Lake Turkana, Kenya (August 22, 2008 to May 17, 2009), at 10-min intervals over 12 d at Gona, Ethiopia (December 8–20, 2008), and at 30-min intervals over 7 mo at the Blackhawk Slide, Lucerne Valley, California (May 23 to December 12, 2009). Temperatures were logged using HOBO Pendant devices, which have a quoted accuracy of ±0.5 °C. These devices were placed at specified depths in narrow trenches (~10 cm wide and 50 cm deep) that were subsequently backfilled with the same soil removed during excavation. Loggers were also placed in shaded environments (under a large, open-air Veranda at Ileret; inside a large, open-air mess tent at Gona; and under the partial shade of an Acacia tree at Gona) to estimate air temperatures. The temperatures recorded by these loggers are regarded as overestimates of free air temperatures because of probable solar-thermal heating of the surrounding structures and due to solar radiation incident on the Acacia tree sensor. At Ileret, loggers were placed at 10-, 26-, 35-, and 50-cm depths in a single soil trench. The vegetative environment was sparse deciduous bush. At Gona, the loggers were placed at 10-, 20-, and 50-cm depths in two different pits, one in an area with sparse grass and another in an area with woody vegetation. At the Blackhawk Slide, loggers were placed at 15-, 30-, and 55-cm depths in a single trench in an area essentially devoid of vegetation. This location was within 300 m of the location where samples were collected for clumped isotope analysis. Locations and summary statistics for these temperature measurements are reported in Table S3. Fig. S1 shows the time-series data from the Blackhawk Slide and Ileret. The soils were relatively dry during the period of temperature measurement at Gona. At the Blackhawk Slide, the soils were slightly moist in May 2009 when the loggers were deployed and were dry when the loggers were retrieved in December 2009, except for the upper ~10 cm that had been wetted during recent rainfall events. At Ileret, the temperature record spans numerous rainfall events, and most of these are associated with a depression in soil temperature (Fig. S1). The subsequent increase in soil temperature following rainfall events is likely related to dewatering of the soils.

**Soil Temperatures in Tropical Environments.** Data were compiled from the literature (1–12) to address the question of how soil temperatures from undisturbed tropical forest habitats (where soils are likely to be fully shaded) compare with those from disturbed forest habitats and naturally open habitats (where soils or near-surface vegetation are likely to receive direct solar radiation). Because our study area is in the tropical low latitudes, this compilation was restricted to nonmontane regions within 12 latitudinal degrees of the equator and was nondiscriminatory with respect to depth of soil temperature measurement, time of day of temperature measurement, or overall duration of study. Because many of the readings were taken from shallow soil depths, the total range of observed temperatures is likely higher than what would be recorded at depth in the soil (i.e., comparable to our isotopic results, which are mostly based on carbonates formed >50 cm below the surface). This bias applies to both undisturbed and disturbed/open localities and thus should not significantly influence the main conclusions relevant to this study, namely, that soil temperatures in undisturbed tropical forest habitats are restricted to a small range averaging near 25 °C and that soil temperatures are typically higher and more variable in disturbed and open habitats. Fig. S2 depicts the results of this compilation.

**Recent Soil Carbonates.** Soil carbonates were collected from soils in Ethiopia, Kenya, China, and the United States. Climate data relevant to these samples are taken from refs. 13–17 and reported in Table S1, and sample information and isotopic results are reported in Table S2. Locations of African soil samples and associated climate stations are plotted in Fig. 1 of the main text, and isotopic temperature data are plotted in Fig. 3 of the main text. All of the African soils are formed in parent material that ultimately derives from igneous (typically volcanic) rock. The ET05-AWSH samples are from an inceptisol formed in a complex of pumaceous gravels and welded tuffs. The samples ET05-AWSH-47 and -48 are ledge-forming and crack-fill soil carbonates. ET05-AWSH-46 is pumice that is impregnated with diffuse carbonate; the anomalous isotopic results for this sample are suggestive of contamination or a mode of formation not representative of typical soil carbonates. The GON07 samples were collected from a soil with minor clay development and dark brown crumbly peds, developed in plateau-forming sands and gravels deposited by the Awash River. The soil carbonates are small nodules (<1 cm diameter). The GONJQ sample is composed of small carbonate nodules collected from a black cotton soil with gilgai relief at the surface formed on a low-relief alluvial fan interfluve. The K2002-MAR sample is an ~4-cm diameter nodule collected from a soil formed in fine-grained sediments along banks of the present-day Mara River.

The BHS samples are from the Blackhawk Slide, Mojave Desert, California. The age of the landslide has been estimated by radiocarbon dating (18) of freshwater gastropods from ponds formed on the surface of the landslide (17,400 ± 550 y B.P.) and by cosmogenic $^{10}$Be exposure age dating (19) of gneissic boulders exposed on the surface of the landslide (24.2 ± 4.8 ka and 5.7 ± 1.1 ka for two different groups of samples). The parent material at our sample locality is a marble breccia with minimal soil development (inceptisol), and the soil carbonates are coatings (pendants) formed on the undersides of parent material clasts. The CN2008 samples are from Damiao, Inner Mongolia, China, and are taken from inceptisols formed in conglomeratic parent material. The samples are both pendant-type carbonates formed on undersides of conglomerate cobbles and nodules formed in fine-grained bank-collapse blocks that were entrained into the conglomerate unit at the time of deposition. This deposit therefore permits a direct comparison between pendant-type and nodular-type carbonate. In both the Blackhawk Slide and the Damiao deposits, the following evidence suggests that these are recent, authigenic carbonates (i.e., several tens of thousands of years in age or younger): (*i*) the pendants and nodules are unique to the soil-forming zone; i.e., an extensive search of underlying, unaltered parent rock revealed no similar carbonate; and (*ii*) the pendants are virtually always found on the undersides of host clasts, rather than in random orientation as would be expected if they formed on host clasts before deposition.

**Paleosol Chronology.** The age of each paleosol horizon was estimated by stratigraphic interpolation between radiometrically dated volcanic tuffs and magnetic reversal events (20–25). There are ≈35 $^{40}$Ar/$^{39}$Ar-dated volcanic horizons in the 4.0- to 0.7-Ma interval in the Turkana Basin, with age uncertainties typically <40 ka for each horizon (22, 23). Thus typical sample age uncertainties are ~40 ka if a uniform sedimentation rate is assumed or ~100 ka if sample ages are simply bracketed between the ages

of overlying and underlying tuffs (the mean and median age differences between dated horizons are 102 and 88 ka, respectively). However, geological evidence suggests that sedimentation occurred continually and at a higher frequency than that of tuff deposition, so in most cases the actual age uncertainties are probably <100 ka (22, 23).

**Laboratory Methods.** Carbon dioxide samples were liberated from carbonates, purified, and introduced to a mass spectrometer using a custom-built, automated, online device. This system (Fig. S3) consists of three coupled systems: (*i*) an autosampler, common acid bath, and cryogenic trap assembly for initial sample digestion, removal of $H_2O$ and other low vapor pressure gases, and collection of $CO_2$; (*ii*) a gas chromatograph (He carrier gas) and cryogenic trap assembly for further purification of $CO_2$; and (*iii*) additional traps and valves to enable the removal of He carrier gas, final cryogenic purification, and expansion of the sample $CO_2$ into the bellows of a mass spectrometer. All system components, including valves, dewar lifters, autosampler, and gas chromatograph, are controlled by custom software written in Labview.

The reaction and purification procedure is carried out as follows. Samples weighed into Ag capsules are loaded into an autosampler (Costech Zero Blank autosampler) and evacuated to <0.5 torr before analysis. Samples are reacted in 100% $H_3PO_4$ at 90 °C for 10 min, and the evolved $H_2O$ and $CO_2$ are removed as the reaction proceeds using dry ice/ethanol and liquid nitrogen traps, respectively (traps A and B in Fig. S3). Following the reaction period, trap B is isolated, incondensable gases are evacuated, and the trap volume is purged by a He carrier gas that flows into the gas chromatograph (25 mL/min). Liquid nitrogen is removed from trap B and replaced with dry ice/ethanol, allowing the sample $CO_2$ to sublimate into the carrier gas stream and pass through the GC and associated cryogenic traps (traps 1a, 1b, and 2). A period of 15 min is given for the sample to completely transit the GC and collect in a liquid nitrogen trap (trap 2) on the downstream side of the column. The GC is a packed column [122 cm length, 3.17 mm o.d., 2.15 mm i.d. (= 4 ft. length, 0.125 in. o.d., 0.085 in. i.d.) Porapak Q 120/80 mesh] and is held at –20 °C throughout the transit interval. Trap 2 is then isolated from the helium flow and evacuated to $\sim 10^{-3}$ torr using the rough pump on the mass spectrometer. The $CO_2$ is cryogenically transferred from trap 2 to trap 3 (5 min; with dry ice/ethanol on trap 2 and liquid nitrogen on trap 3), then allowed to expand within the restricted volume of trap 3 by removing liquid nitrogen (5-min expansion period), and finally expanded into the bellows of the mass spectrometer (2-min transfer period). During standby, the GC column is held at 100 °C and subjected to reverse carrier gas flow to purge contaminants, while other components of the system, including the autosampler and acid bath assembly, are held under vacuum.

All isotope ratios in this study were determined using a ThermoFinnigan MAT 253 mass spectrometer at Caltech (Caltech no. 2 instrument), which has a collector configuration similar to the Caltech no. 1 instrument described in earlier studies (26). Each extracted $CO_2$ sample was analyzed at a signal intensity of 16 V (44-cup) over eight acquisitions, for a total ion collection period of 1,456 s each for sample and reference gas (2,912 s total; seven cycles per acquisition, 26-s counting period per gas per cycle). On this mass spectrometer, we replaced the stock stainless steel capillary tubes with VICI electroformed nickel (EFNi) capillaries [122 cm, 0.794 mm o.d., 0.127 mm i.d. (= 4 ft. length, 1/32 in. o.d., 0.005 in. i.d.)]. Extensive investigation in our lab traced isotope redistribution reactions (i.e., reactions of the type $^{13}C^{18}O^{16}O + {}^{12}C^{16}O^{16}O \rightarrow {}^{13}C^{16}O^{16}O + {}^{12}C^{18}O^{16}O$), and thus alteration of 47/44, to stainless steel capillaries. Although not all stainless steel capillaries give rise to redistribution reactions, none of the EFNi capillary pairs that we have installed so far at Caltech ($n = 3$) have induced measurable redistribution, and no baking or other preconditioning of the capillaries was necessary to achieve this. We speculate that stainless steel in general, or at least the stainless steel used to manufacture ThermoFinnigan capillaries, is in some cases catalytically active, or has a high surface area that harbors water, or both, whereas these effects are minimized in electropolished nickel capillaries.

**Data Reduction and Normalization.** The parameter $\Delta_{47}$ is calculated as

$$\Delta_{47} = \left[\left(\frac{R^{47}}{R^{47*}} - 1\right) - \left(\frac{R^{46}}{R^{46*}} - 1\right) - \left(\frac{R^{45}}{R^{45*}} - 1\right)\right] \times 1000 \quad \textbf{[S1]}$$

(27), where

$$R^i = \frac{\text{mass } i}{\text{mass } 44}. \quad \textbf{[S2]}$$

The parameter $R^{i*}$ is analogous to $R^i$, but corresponds to the stochastic distributions of masses 47, 46, and 45. Calculation of $R^{i*}$ is introduced in ref. 26 and detailed in ref. 27. In addition,

$$\delta 47_{SA\text{–}WG} = \left(\frac{R^{47}_{SA}}{R^{47}_{WG}} - 1\right) \times 1000, \quad \textbf{[S3]}$$

where the subscripts SA and WG refer to the sample $CO_2$ and the working gas $CO_2$, respectively.

Raw data were corrected for instrument nonlinearity, scale compression, and acid reaction temperature and were then normalized to working carbonate standards run along with the unknowns. The procedure is summarized as follows:

(*i*) Correct for instrument nonlinearity by normalizing sample $\Delta_{47}$ to a "heated gas line" (28) evaluated at $\delta 47_{\text{SA-WG}}$,

$$\Delta_{47,SA\text{–}HG} = \Delta_{47,SA\text{–}WG} - \Delta_{47,HG\text{–}WG}, \quad \textbf{[S4]}$$

where

$$\Delta_{47,HG\text{–}WG} = m * \delta 47_{SA\text{–}WG} + b \quad \textbf{[S5]}$$

and where $m$ and $b$ are the slope and intercept of a heated gas line (28), and $\Delta_{47,\text{SA-WG}}$ is the raw $\Delta_{47}$ value of the sample relative to the working gas. The concept of normalization to heated gases was introduced by Eiler and Shauble (26), and the heated gas line concept is reviewed in detail in Huntington et al. (28). In this study, pervasive drift in the slope and intercept of the heated gas line made it necessary to model $m$ and $b$ as low-order polynomial functions of sample order number $n$ using a least-squares approach (see *Moving Heated Gas Line* section below). For such a time-transient or "moving" heated gas line, Eq. **S5** becomes

$$\Delta_{47,HG\text{–}WG} = m(\text{n})\,\delta 47_{SA\text{–}WG} + b(\text{n}). \quad \textbf{[S6]}$$

(*ii*) Correct for "scale compression" (28) by multiplying $\Delta_{47,\text{SA-HG}}$ by a factor proportional to the intercept of the heated gas line,

$$\Delta_{47,SA\text{–}HG,uncompressed} = \Delta_{47,SA\text{–}HG} \times \frac{-0.8453}{b(\text{n})}, \quad \textbf{[S7]}$$

where the value −0.8453 is the heated gas line intercept (vs. Ozetch working gas $CO_2$) that characterized the Caltech Ther-

mo MAT 253 no. 1 instrument during the development of the $T - \Delta_{47}$ calibration reported in Ghosh et al. (29). This scale compression, as discussed in ref. 28, may relate to factors that vary between different instruments (or over the course of time for a single instrument), for example the source pressure, residence time of molecules in the source, and electron energy, that lead to subtle differences in compression/expansion of the $\Delta_{47}$ scale. Implicit in the use of the −0.8453‰ intercept is the assumption that different batches of Oztech working gas have identical $\Delta_{47}$ compositions.

(*iii*) Correct for the difference in phosphoric acid temperature between that used for this study (90 °C) and that used for the inorganic calibration of Ghosh et al. (29) (25 °C),

$$\Delta_{47,SA\text{–}HG,acid} = \Delta_{47,SA\text{–}HG,uncompressed} + 0.081, \quad \textbf{[S8]}$$

where the 0.081‰ correction factor is based on replicate 90 °C extractions of two materials traceable to the original calibration (29): NBS-19 ($\Delta_{47}$ = 0.352‰), and speleothem 2-8-E (0.641‰; Affek et al., ref. 30) (Table S5). This offset is similar to that observed for other in-house "working" carbonate standards and is used as a correction factor applied to all calcium carbonate samples analyzed using the online 90 °C system. This value is similar but not equivalent to the theoretical difference of 0.069‰ given by equation 23 in Guo et al. (31).

(*iv*) Normalize to working carbonate standards with previously determined $\Delta_{47}$. These are prepared, analyzed, and normalized to heated gases, in exactly the same manner as the unknowns; their $\Delta_{47}$ residuals from accepted values are used to make final run-specific $\Delta_{47}$ corrections (usually <0.02‰) that account for variability in components of the preparation system not seen by heated gas samples, including the acid reaction environment. To have confidence in such a correction, the residuals of different standards should be similar during any specific time interval. For example, there should be no correlation between $\Delta_{47}$ residuals and the nominal δ47 or $\Delta_{47}$ values of different standards, as such correlation would indicate an incorrect heated gas line slope or "stretching factor" assumed as part of the normalization to heated gas data. For this study, corrections were determined by fitting polynomial functions of sample order number n to the $\Delta_{47}$ residuals of standards (Fig. S4 and Dataset S1).

In addition, 48/44 ion ratios were measured as a part of each analysis, which permitted calculation of the parameter $\Delta_{48,SA\text{-}HG}$. This parameter is analogous to $\Delta_{47,SA\text{-}HG}$ and is the difference between the measured signal at mass 48 and that predicted for a stochastic distribution of isotopologues. This parameter was used to monitor for contamination, as the signal deriving from mass 48 $CO_2$ isotopologues is minute and easily overwhelmed by contaminants at $m/z$ = 48. $\Delta_{48,SA\text{-}HG}$ was <1‰ in magnitude for all soil carbonates examined in this study (Dataset S1), and no $\Delta_{47}$ data were rejected on the basis of $\Delta_{48,SA\text{-}HG}$.

$\delta^{13}C$ and $\delta^{18}O$ values were normalized relative to NBS-19 ($\delta^{13}C$ = 1.95‰ V-PDB, $\delta^{18}O$ = −2.19‰ V-PDB) and to working carbonate standards calibrated to NBS-19. A fractionation factor of 1.0082 (90 °C) was used to account for the temperature-dependent oxygen isotope fractionation between $CO_2$ gas and mineral resulting from the reaction in phopsphoric acid (32). The oxygen isotopic composition of water in equilibrium with soil carbonates was calculated using the relation

$$1000\ln\alpha = 18.03\left(10^3 T^{-1}\right) - 32.42 \quad \textbf{[S9]}$$

(33), where

$$\alpha = \frac{1000 + \delta^{18}O_{carb}}{1000 + \delta^{18}O_{water}}. \quad \textbf{[S10]}$$

Error in the calculated $\delta^{18}O_{water}$ value was determined by propagating the errors in temperature (inferred from $\Delta_{47}$) and $\delta^{18}O_{carb}$ through these equations.

**Moving Heated Gas Line.** In the case where the instrument nonlinearity changes as a function of time or sample throughput, the corresponding movement of the heated gas line may be modeled as a time-dependent (or cumulative sample number-dependent) variable. In practice, we have found that if active, the heated gas line movement is more strongly related to the cumulative sample throughput rather than being a simple function of time. In addition, the movement of the heated gas line is often gradual and follows a predictable trajectory such that the slope and intercept of the heated gas line can be modeled, for example, as low-order polynomial functions of sample order number.

For this study, we developed an inverse procedure for modeling the movement of the heated gas line, as constrained by numerous heated gas observations $\Delta_{47i,obs}$, $\delta47_{i,obs}$. The "position" of the heated gas line at any instant is completely described by its slope and intercept:

$$\Delta_{47i} = m_i \delta 47_i + b_i. \quad \textbf{[S11]}$$

The slope $m$ and intercept $b$ of this line change as a function of the sample order number $t$ (e.g., for the first sample analyzed, $t$ = 1; for the fifth, $t$ = 5; and so on) is here modeled as a second-order polynomial:

$$m_i = xt_i^2 + yt_i + z \quad \textbf{[S12]}$$

$$b_i = jt_i^2 + kt_i + l. \quad \textbf{[S13]}$$

Combining Eqs. **S11**, **S12**, and **S13**,

$$\Delta_{47i} = \left(xt_i^2 + yt_i + z\right)\delta47_i + \left(jt_i^2 + kt_i + l\right). \quad \textbf{[S14]}$$

Expanding this into matrix notation yields

$$\begin{bmatrix} \delta47_i t_i^2 & \delta47_i t_i & \delta47_i & t_i^2 & t_i & 1 \\ \delta47_i t_{i+1}^2 & \delta47_i t_{i+1} & \delta47_{i+1} & t_{i+1}^2 & t_{i+1} & 1 \\ . & . & . & . & . & . \\ . & . & . & . & . & . \\ \delta47_i t_n^2 & \delta47_i t_n & \delta47_n & t_n^2 & t_n & 1 \end{bmatrix} * \begin{bmatrix} x \\ y \\ z \\ j \\ k \\ l \end{bmatrix} = \begin{bmatrix} \Delta_{47i} \\ \Delta_{47i+1} \\ . \\ . \\ \Delta_{47n} \end{bmatrix}. \quad \textbf{[S15]}$$

If we substitute the $\delta47_i$ and $\Delta_{47i}$ parameters with heated gas observations $\delta47_{i,obs}$, $\Delta_{47i,obs}$, then the only unknown variables are represented by the column vector **m** on the left-hand side of the equation (i.e., $\mathbf{m} = [x\ y\ z\ j\ k\ l]^T$), and given more than six heated gas observations, the linear system is overdetermined and **m** can be estimated using a least-squares solution

$$\mathbf{m_{est}} = \left(\mathbf{A^T A}\right)^{-1}\mathbf{A^T d} \quad \textbf{[S16]}$$

(34), where **A** is the matrix on the left-hand side of Eq. **S15**, and **d** is the column vector on the right-hand side of Eq. **S15**. Finally, the solution is evaluated by computing

$$\mathbf{d_{pred}} = \mathbf{A m_{est}}, \quad \textbf{[S17]}$$

where $\mathbf{d_{pred}}$ is a column vector containing the predicted $\Delta_{47}$ residuals of the heated gases. These residuals should have a mean

value of zero, but with a SD around the mean that is consistent with the external precision of heated gas analyses (~0.015‰). If the SD is significantly lower or higher than this value, then the choice of polynomial order for modeling the heated gas line movement resulted in overprediction or underprediction of the system (34), respectively, and a new value must be chosen. In practice, polynomials of order 1, 2, and 3 are typically sufficient to model the heated gas line movement; if higher orders seem necessary, then the system is likely ill posed, for instance, because the heated gas line movement is nonsystematic or spans discontinuities such as those that can occur following major equipment failure or routine maintenance.

**Estimation of Uncertainty.** At shot-noise limits, our 16-V, 1,456-s integration time analyses should produce a population of $\Delta_{47}$ values with a 1σ precision of 0.009‰ (calculated using equation 15 in ref. 35). Over the course of this study, the observed 1σ precisions ranged between 0.009 and 0.019‰ for carbonate materials extracted multiple times (Table S5) and an average 1σ precision of 0.0124‰ for East African paleosol carbonates extracted multiple times. This observation of slightly lower external precision compared with internal precision is consistent with previous observations in our laboratory and likely owes to a combination of sample heterogeneity and slight variation in reaction, extraction, and mass spectrometer conditions from sample to sample (28).

The uncertainties reported in Tables S2 and S4, and the error bars shown in Figs. 3 and 4, were derived as follows. For $n = 1$ (that is, samples extracted from carbonate once), uncertainty in $\Delta_{47}$ was taken as the SEM $\Delta_{47}$ value over eight acquisitions or as the observed external precision for paleosol carbonates (= 0.0124‰), whichever is higher. This uncertainty was then combined with the uncertainty in the acid temperature correction (0.0024‰) using SE propagation procedures. The nominal uncertainty for $n = 1$ is 0.013‰, unless otherwise noted in Tables S2 and S4. For $n = 2$, uncertainty was taken as the SEM $\Delta_{47}$ value over 16 acquisitions, combined with the uncertainty in the acid temperature correction (0.0024‰). For $n \geq 3$, uncertainty was taken as the SEM $\Delta_{47}$ value of all extractions, combined with the uncertainty in acid temperature correction (0.0024‰).

For calculation of temperature uncertainty, an uncertainty in $\Delta_{47}$ of 0.005‰ is estimated for the $\Delta_{47}$ temperature equation (29). Note that whereas this error estimate is commensurate with the data in ref. 29, ongoing calibration studies are in agreement with the temperature equation in ref. 29 and have significantly reduced the associated margin of error. Regardless, the 0.005‰ uncertainty estimate was combined with the uncertainty in $\Delta_{47}$, as determined above, and then propagated through the $\Delta_{47}$ temperature equation to derive upper and lower temperature estimates from which the temperature uncertainties reported in Tables S2 and S4 were derived.

**Analytical Summary.** Samples were analyzed during April through October 2008 and during January 2009. A change of the mass spectrometer source filament near the end of September 2008 resulted in a discontinuity in the drift of the heated gas line, and samples analyzed during April through September, and those analyzed during October, were normalized using separate moving heated gas line models. The January 2009 data were normalized relative to a fixed heated gas line model. Dataset S1 reports δ47, $\Delta_{47}$, δ48, and $\Delta_{48}$ data for samples relevant to this study, along with all heated gases and standards used to normalize the data (equaling all heated gases and standards analyzed during the period of study, with the exception of a small number of observations with exotic δ47 compositions far outside of the range relevant to this study and observations removed because of known or suspected errors in sample preparation or analysis). The external precision of carbonate standards ranged between 0.009 and 0.019‰ for different materials (Table S5). The precision for carbonate standards ranges between 0.008 and 0.011‰ after self-normalization for temporally coherent residuals. The normalizations are based on 10th-, fourth-, and first-order polynomials fitted to working standard $\Delta_{47}$ residuals for the April–September, October, and January data, respectively, and the magnitude of the correction for each sample is reported in Dataset S1.


1. Anikwe MAN, Ubochi JN (2007) Short-term changes in soil properties under tillage systems and their effect on sweet potato (*Ipomea batatas* L.) growth and yield in an Ultisol in south-eastern Nigeria. *Aust J Soil Res* 45:351–358.
2. Gut A, et al. (2002) NO emission from an Amazonian rain forest soil: Continuous measurements of NO flux and soil concentration. *J Geophys Res*, 107:D20, 8057.
3. Kosugi Y, et al. (2007) Spatial and temporal variation in soil respiration in a Southeast Asian tropical rainforest. *Agric For Meteorol* 147:35–47.
4. Marthews TR, Burslem DFRP, Paton SR, Yanguez F, Mullins CE (2008) Soil drying in a tropical forest: Three distinct environments controlled by gap size. *Ecol Modell* 216:369–384.
5. Melling L, Hatano R, Goh KJ (2007) Nitrous oxide emissions from three ecosystems in tropical peatland of Sarawak, Malaysia. *Soil Sci Plant Nutr* 53:792–805.
6. Murphy M, Balser T, Buchmann N, Hahn V, Potvin C (2008) Linking tree biodiversity to belowground process in a young tropical plantation: Impacts on soil $CO_2$flux. *For Ecol Manage* 255:2577–2588.
7. Passianoto CC, et al. (2004) Diurnal changes in nitric oxide emissions from conventional tillage and pasture sites in the Amazon Basin: Influence of soil temperature. *Plant Soil* 258:21–29.
8. Saraswathi SG, Lalrammawia C, Paliwal K (2008) Seasonal variability in soil-surface $CO_2$ efflux in selected young tree plantations in semi-arid eco-climate of Madurai. *Curr Sci* 95:94–99.
9. Schwendenmann L, Veldkamp E (2006) Long-term $CO_2$production from deeply weathered soils of a tropical rain forest: Evidence for a potential positive feedback to climate warming. *Glob Change Biol* 12:1878–1893.
10. Sotta E, et al. (2004) Soil $CO_2$ efflux in a tropical forest in the central Amazon. *Glob Change Biol* 10:601–617.
11. Valentini CMA, Espinosa MM, de Paulo SR (2008) Estimate of $CO_2$ efflux of soil, of a transition forest in northwest of Mato Grosso State, using multiple regression. *Cerne, Lavras* 14:9–16.
12. Yashiro YK, Kadir WR, Okuda T, Koizumi H (2008) The effects of logging on soil greenhouse gas ($CO_2$, $CH_4$, $N_2O$) flux in a tropical rain forest, Peninsular Malaysia. *Agric For Meteorol* 148:799–806.
13. Global Climate Observing System, National Climatic Data Center, NOAA, US Department of Commerce Available at http://www.gosic.org/GCOS/GSN/GSNdatamatrix.htm Accessed August 2006.
14. National Meteorological Agency of Ethiopia (Addis Abbaba, Ethiopia.) Available at http://www.ethiomet.gov.et/ Accessed January 2004.
15. East African Meteorological Department (1975) *Climatological Statistics for East Africa* (East African Meteorological Department, Nairobi, Kenya).
16. University Corporation for Atmospheric Research (2006) *China Monthly Station Precipitation and Temperature, 1951-1990*. Available at http://dss.ucar.edu/datasets/ds578.1 Accessed August 2006.
17. Western regional Climate Center (2009) *Western Regional Climate Center*, http://www.wrcc.dri.edu/cgi-bin/cliMAIN.pl?ca5182. Accessed March 2009.
18. Stout M (1975) Age of the Blackhawk landslide, southern California. *Abstracts with Programs, Geol Soc Am* 7:378–379.
19. Nichols K, Bierman P, Caffee M (2000) The Blackhawk keeps its secrets: Landslide dating using in situ 10-Be. *Abstracts with Programs, Geol Soc Am* 32:400.
20. Kidane T, Otofuji Y-I, Brown FH, Takemoto K, Eshete G (2007) Two normal paleomagnetic polarity intervals in the lower Matuyama Chron recorded in the Shungura Formation (Omo Valley, Southwest Ethiopia). *Earth Planet Sci Lett* 262:240–256.
21. deMenocal PB, Brown FH (1999) *Pliiocene tephra correlations between East African hominid localities, the Gulf of Aden, and the Arabian Sea. The Evolution of Neogene Terrestrial Ecosystems in Europe*, eds Agusti J, Rook L, Andrews P (Cambridge University Press, Cambridge, UK).
22. McDougall I, Brown FH (2006) Precise $^{40}Ar/^{39}Ar$ geochronology for the upper Koobi Fora Formation, Turkana Basin, northern Kenya. *J Geol Soc Lond* 163:205–220.
23. McDougall I, Brown FH (2008) Geochronology of the pre-KBS Tuff sequence, Omo Group, Turkana Basin. *J Geol Soc Lond* 165:549–562.
24. Brown FH, Sarna-Wojcicki AM, Meyer CE, Haileab B (1992) Correlation of Pliocene and Pleistocene tephra layers between the Turkana Basin of East Africa and the Gulf of Aden. *Quat Int* 13/14:55–67.
25. Feibel CS, Brown FH, McDougall I (1989) Stratigraphic context of fossil hominids from the Omo Group deposits: Northern Turkana Basin, Kenya and Ethiopia. *Am J Phys Anthropol* 78:595–622.
26. Eiler J, Schauble E (2004) $^{18}O^{13}C^{16}O$ in Earth's atmosphere. *Geochim Cosmochim Acta* 68:4767–4777.
27. Affek HP, Eiler JM (2006) Abundance of mass 47 $CO_2$ in urban air, car exhaust, and human breath. *Geochim Cosmochim Acta* 70:1–12.
28. Huntington K, et al. (2009) Methods and limitations of analyses of 'clumped' CO2 isotopes ($\Delta_{47}$) by gas source isotope ratio mass spectrometry. *J Mass Spectrom* 44:1318–1329.

29. Ghosh P, et al. (2006) $^{13}C$-$^{18}O$ bonds in carbonate minerals: A new kind of paleothermometer. *Geochim Cosmochim Acta* 70:1439–1456.
30. Affek HP, Bar-Matthews M, Ayalon A, Matthews A, Eiler JM (2008) Glacial/interglacial temperature variations in Soreq cave speleothems as recorded by 'clumped isotope' thermometry. *Geochim Cosmochim Acta* 72:5351–5360.
31. Guo W, Mosenfelder JL, Goddard WAI, Eiler JM (2009) Isotopic fractionations associated with phosphoric acid digestion of carbonate minerals: Insights from first-principles theoretical modeling and clumped isotope measurements. *Geochim Cosmochim Acta* 73:7203–7225.
32. Swart PK, Burns SJ, Leder JJ (1991) Fractionation of stable isotopes of oxygen and carbon in carbon dioxide during the reaction of calcite with phosphoric acid as a function of temperature and technique. *Chem Geol Isot Geosci Sec* 86:89–96.
33. Kim S-T, O'Neil JR (1997) Equilibrium and nonequilibrium oxygen isotope effects in synthetic carbonates. *Geochim Cosmochim Acta* 61 (16):3461–3475.
34. Menke W (1989) *Geophysical Data Analysis: Discrete Inverse Theory* (Academic Press).
35. Merritt DA, Hayes JM (1994) Factors controlling precision and accuracy in isotope-ratio-monitoring mass spectrometry. *Anal Chem* 66:2336–2347.

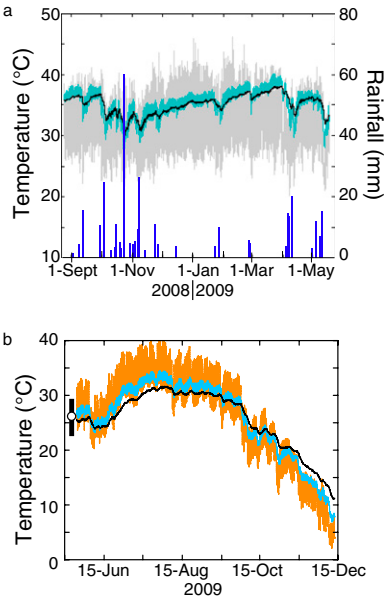


**Fig. S1.** (*a*) Air temperature, soil temperature, and rainfall records at Ileret, Marsabit District, Kenya. Gray, aqua, and black fields show air temperature, 26-cm-depth soil temperature, and 50-cm-depth soil temperature, respectively. Blue lines show rainfall amount. The average air temperature during this interval was 31.3 °C, whereas the average ground temperature (50 cm) was 35.2 °C. (*b*) Soil temperatures measured at the Blackhawk Slide, Lucerne Valley, California during May–December 2009. Black, aqua, and orange lines are soil temperatures at 55-, 30-, and 15-cm depths below the soil surface, respectively. The circle and error bar on the left indicate the average and SD of clumped isotope temperatures of soil carbonates collected from the Blackhawk Slide (Table S2).

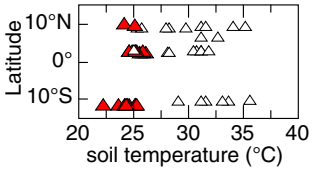


**Fig. S2.** Low latitude soil temperatures. Red triangles are soils from primary tropical rainforest; white triangles are soils from disturbed areas (canopy gaps, pasture, tree plantations, logged forest) or naturally open habitat. Data are taken from refs. 1–12.

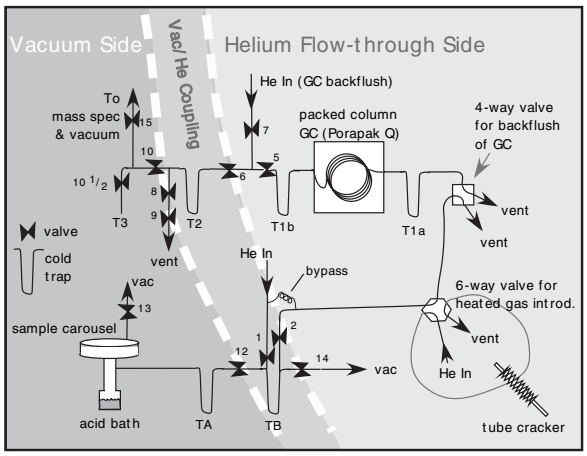


**Fig. S3.** Schematic diagram of the online carbonate extraction apparatus used in this study. Abbreviations: GC, gas chromatograph; T, trap (e.g., TA, trap A); vac, vacuum.

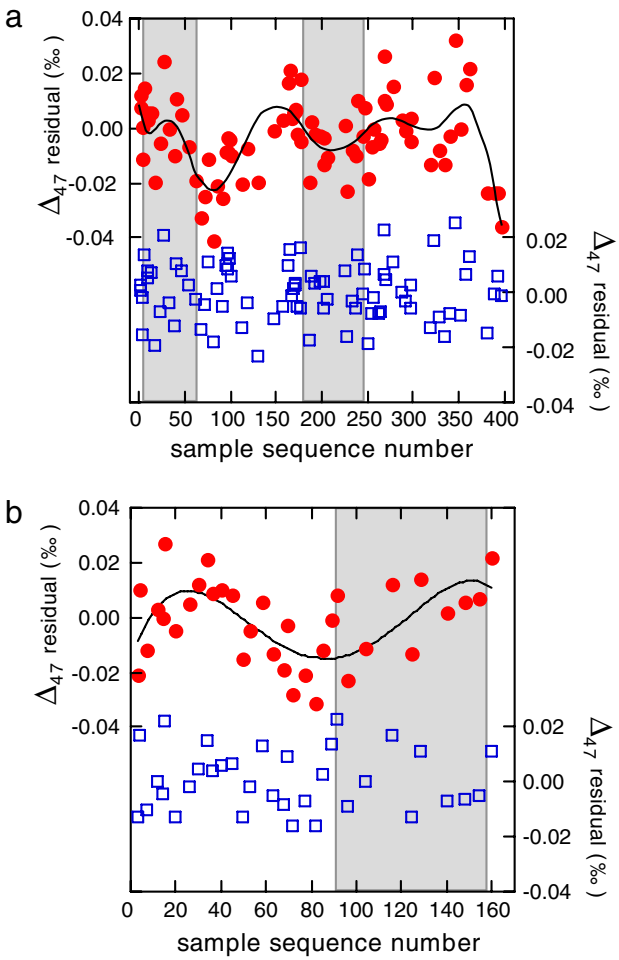


**Fig. S4.** Temporal variation in $\Delta_{47}$ residuals of carbonate standards. (*a*) April through September 2008 analytical series. (*b*) October 2008 series. Red circles are residuals of carbonate standards from accepted values. Black lines are 10th- and fourth-order polynomial fits to residuals for April–September and October data, respectively. Open blue squares show the residuals after normalization to the polynomial fit. Shaded regions show time intervals during which samples for this study were analyzed. All data are reported in Dataset S1.

**Table S1. Climate data relevant to this study**

| Site, mo | Mean temperature, °C | Precipitation, mm | Site, mo | Mean temperature, °C | Precipitation, mm |
|---|---|---|---|---|---|
| Narok, Kenya; 1.13 S, 35.83 E, 1,890 m | | | Hohot, China, 40.8 N, 111.7 E, 1,063 m | | |
| January | 17.2 | 74 | January | −12.7 | 2.8 |
| February | 17.4 | 79 | February | −8.7 | 6.0 |
| March | 17.5 | 103 | March | −0.2 | 10.0 |
| April | 17.7 | 144 | April | 8.2 | 17.5 |
| May | 17.0 | 94 | May | 15.6 | 26.6 |
| June | 15.4 | 27 | June | 20.3 | 44.9 |
| July | 14.8 | 15 | July | 22.2 | 100.3 |
| August | 15.1 | 20 | August | 20.1 | 127.2 |
| September | 15.9 | 22 | September | 14.0 | 45.9 |
| October | 16.8 | 25 | October | 6.7 | 22.5 |
| November | 16.7 | 62 | November | −2.7 | 6.3 |
| December | 16.8 | 71 | December | −10.7 | 1.3 |
| Annual | 16.5 | 736 | Annual | 6.0 | 411.2 |
| Warmest 3 mo | 17.5 | — | Warmest 3 mo | 20.8 | — |
| Awash, Ethiopia: 8.93 N, 40.08 E, 1,052 m | | | Lucerne Valley, California: 34.4 N, 117.0 W, 921 m | | |
| January | 25.2 | — | January | 5.6 | 11.4 |
| February | 26.1 | — | February | 9.0 | 8.6 |
| March | 28.3 | — | March | 12.4 | 8.4 |
| April | 28.7 | — | April | 14.5 | 3.0 |
| May | 29.4 | — | May | 18.3 | 1.8 |
| June | 30.6 | — | June | 23.8 | 0.5 |
| July | 28.3 | — | July | 27.7 | 6.4 |
| August | 27.7 | — | August | 25.9 | 23.1 |
| September | 27.8 | — | September | 21.0 | 2.5 |
| October | 27.8 | — | October | 13.9 | 6.6 |
| November | 26.0 | — | November | 7.5 | 14.5 |
| December | 25.4 | — | December | 4.2 | 18.5 |
| Annual | 27.6 | — | Annual | 15.3 | 105.4 |
| Warmest 3 mo | 29.6 | — | Warmest 3 mo | 25.8 | — |
| Mile, Ethiopia: 11.42 N, 40.75 E, 420 m | | | Lodwar, Kenya: 3.1 N, 35.6 E, 506 m | | |
| January | 26.5 | — | January | 28.7 | 9 |
| February | 27.0 | — | February | 29.7 | 7 |
| March | 29.0 | — | March | 30.1 | 21 |
| April | 30.7 | — | April | 29.5 | 48 |
| May | 33.0 | — | May | 29.7 | 25 |
| June | 35.3 | — | June | 29.0 | 7 |
| July | 33.0 | — | July | 28.3 | 14 |
| August | 32.0 | — | August | 28.4 | 10 |
| September | 32.8 | — | September | 29.4 | 3 |
| October | 30.4 | — | October | 29.8 | 8 |
| November | 27.5 | — | November | 29.0 | 13 |
| December | 26.4 | — | December | 28.5 | 13 |
| Annual | 30.3 | — | Annual | 29.2 | 178 |
| Warmest 3 mo | 33.8 | — | Warmest 3 mo | 29.7 | — |

Data sources: Awash, Ethiopia, ref. 13; Mile, Ethiopia, ref. 14; Lodwar, Kenya and Narok, Kenya, ref. 15; Hohot, China, ref. 16; Lucerne Valley, California, ref. 17.

**Table S2. Summary of stable isotope data for soil carbonates collected from recent soils**

| Site, sample no. | Climate station[†] | MAT, °C[‡] | MWST, °C[‡] | Type | Depth, cm[§] | $N$[¶] | $\delta^{13}C_c$, ‰, PDB[‖] | $\delta^{18}O_c$, ‰, PDB[‖] | $\Delta_{47}$, ‰, HG[††] | Temp., °C[‡‡] | $\delta^{18}O_{sw}$, SMOW[§§] |
|---|---|---|---|---|---|---|---|---|---|---|---|
| Awash, Ethiopia: 8.788395 N, 39.66166 E, 1,259 m | | | | | | | | | | | |
| ET05-AWSH-47-1 | Awash | 26.4 | 28.2 | Ledge | 280 | 1 | −0.6 | −5.7 | 0.638 | 26.8 (3.1) | −3.0 |
| ET05-AWSH-48-1 | Awash | 26.4 | 28.2 | Crack fill | 130 | 1 | 0.5 | −5.0 | 0.645 | 25.2 (3.1) | −2.6 |
| Gona, Ethiopia: 11.148123 N, 40.33566 E, 694 m | | | | | | | | | | | |
| GONJQ-305-1 | Mile | 28.7 | 32.1 | Nodule | 50 | 2 | −2.5 | −5.5 | 0.628 (0.008) | 29.1 (2.4) | −2.4 (0.5) |
| Gona, Ethiopia: 11.16525 N, 40.49496 E, 637 m | | | | | | | | | | | |
| GON07-4.3-1 | Mile | 29.0 | 32.5 | Nodule | 13 | 1 | −0.2 | −2.3 | 0.600 | 35.9 (3.4) | 2.2 |
| GON07-4.4-1 | Mile | 29.0 | 32.5 | Nodule | 21 | 1 | −1.1 | −3.6 | 0.605 | 34.6 (3.3) | 0.6 |
| GON07-4.5-1 | Mile | 29.0 | 32.5 | Nodule | 28 | 1 | −1.0 | −2.0 | 0.616 | 32.0 (3.2) | 1.7 |
| GON07-4.6-1 | Mile | 29.0 | 32.5 | Nodule | 35 | 1 | −1.2 | −3.0 | 0.633 | 27.9 (3.1) | −0.1 |
| GON07-4.6-2 | Mile | 29.0 | 32.5 | Nodule | 35 | 1 | −2.9 | −2.0 | 0.582 | 40.3 (3.5) | 3.3 |
| GON07-4.7-1 | Mile | 29.0 | 32.5 | Nodule | 45 | 2 | −1.5 | −3.5 | 0.629 (0.009) | 28.9 (2.4) | −0.4 (0.5) |
| Masai Mara, Kenya: 1.5466 S, 35.0234 E, 1,477 m | | | | | | | | | | | |
| K2002-MAR-103-1 | Narok | 19.0 | 20.2 | Nodule | — | 2 | 0.8 | −3.0 | 0.674 (0.005) | 18.8 (1.6) | −1.9 (0.3) |
| Damiao, Inner Mongolia, China: 42.01528 N, 111.5743 E, 1,306 m | | | | | | | | | | | |
| CN2008-DM-165-1 | Hohot | 4.6 | 19.4 | Nodule | 60 | 1 | −5.3 | −7.3 | 0.652 | 23.7 (3.0) | −5.2 |
| CN2008-DM-166-1 | Hohot | 4.6 | 19.4 | Nodule | 60 | 1 | −5.5 | −8.6 | 0.646 | 24.9 (3.0) | −6.3 |
| CN2008-DM-169-2 | Hohot | 4.6 | 19.4 | Pendant | 65 | 1 | −3.8 | −7.6 | 0.673 | 19.2 (2.9) | −6.5 |
| CN2008-DM-169-1 | Hohot | 4.6 | 19.4 | Nodule | 65 | 1 | −5.5 | −8.9 | 0.660 | 21.9 (2.9) | −7.2 |
| CN2008-DM-164-20cm-1 | Hohot | 4.6 | 19.4 | Pendant | 20 | 1 | −3.0 | −8.6 | 0.626 | 29.6 (3.2) | −5.4 |
| CN2008-DM-164-30cm-1 | Hohot | 4.6 | 19.4 | Pendant | 30 | 1 | −1.8 | −7.7 | 0.648 | 24.7 (3.0) | −5.4 |
| CN2008-DM-164-40cm-1 | Hohot | 4.6 | 19.4 | Pendant | 40 | 1 | −4.0 | −7.9 | 0.629 | 28.8 (3.1) | −4.8 |
| CN2008-DM-164-50cm-1 | Hohot | 4.6 | 19.4 | Pendant | 50 | 1 | −3.7 | −8.0 | 0.691 | 15.3 (2.8) | −7.7 |
| CN2008-DM-164-80cm-1 | Hohot | 4.6 | 19.4 | Pendant | 80 | 1 | −4.9 | −9.4 | 0.647 | 24.8 (3.0) | −7.1 |
| CN2008-DM-164-100cm-1 | Hohot | 4.6 | 19.4 | Pendant | 100 | 1 | −4.6 | −8.8 | 0.638 | 26.8 (3.1) | −6.1 |
| CN2008-DM-164-120cm-1 | Hohot | 4.6 | 19.4 | Pendant | 120 | 2 | −3.9 | −8.2 | 0.696 (0.006) | 14.4 (1.6) | −8.1 (0.4) |
| CN2008-DM-164-130cm-1 | Hohot | 4.6 | 19.4 | Pendant | 130 | 1 | −3.0 | −7.6 | 0.653 | 23.4 (3.0) | −5.6 |
| Blackhawk Slide, Mojave Desert, California: 34.42119 N, 116.789 W, 982 m | | | | | | | | | | | |
| CA08-BHS-006.1 | Lucerne | 15.0 | 25.4 | Pendant | Surface | 1 | −1.5 | −7.4 | 0.641 (0.016) | 26.0 (3.8) | −4.9 (0.8) |
| CA08-BHS-001.1 | Lucerne | 15.0 | 25.4 | Pendant | 35 | 2 | −3.1 | −8.5 | 0.637 (0.008) | 27.0 (2.3) | −5.8 (0.5) |
| CA08-BHS-002.1 | Lucerne | 15.0 | 25.4 | Pendant | 55 | 3 | −4.4 | −10.0 | 0.647 (0.006) | 24.8 (1.8) | −7.7 (0.4) |
| CA08-BHS-003.1 | Lucerne | 15.0 | 25.4 | Pendant | 80 | 3 | −4.4 | −9.6 | 0.659 (0.006) | 22.2 (1.8) | −7.9 (0.4) |
| CA08-BHS-004.1 | Lucerne | 15.0 | 25.4 | Pendant | 110 | 2 | −2.2 | −10.8 | 0.618 (0.010) | 31.5 (2.8) | −7.2 (0.5) |
| CA08-BHS-005.1 | Lucerne | 15.0 | 25.4 | Pendant | 140 | 2 | −3.4 | −10.2 | 0.646 (0.009) | 24.9 (2.5) | −7.9 (0.5) |
| Associated carbonates | | | | | | | | | | | |
| CA08-BHS-001.3 | Lucerne | 15.0 | 25.4 | Marble | — | 1 | 4.1 | −9.3 | 0.383 (0.017) | 110.0 (8.5) | 6.4 (1.0) |
| ET05-AWSH-46–1 | Awash | 26.4 | 28.2 | $CaCO_3$ in pumice | | 1 | −5.2 | 5.5 | 0.584 | 40.0 (3.5) | 10.8 (0.7) |

[†]Climate data are reported in Table S1.

[‡]MAT, mean annual temperature; MWST, mean warm season temperature (mean temperature of the three warmest consecutive months). These data are corrected for elevation differences between sample localities and nearest climate stations, using a 6 °C/km lapse rate.

[§]Depth at which the carbonates were sampled relative to the present soil surface.

[¶]Number of unique analyses, where each analysis involves extraction of $CO_2$ from carbonate, and isotope ratio measurement over eight acquisitions in the mass spectrometer, as described in the text.

[‖]The subscript "c" denotes carbonate. PDB: Pee Dee belemnite. Replicate extraction-level uncertainty in $\delta^{13}C$ and $\delta^{18}O$ is <0.07‰ and 0.06‰, respectively.

[††]HG, heated gas. Uncertainty is 0.013‰ unless otherwise noted in parentheses.

[‡‡]Calculated using the $\Delta_{47} - T$ relationship of Ghosh (1). The uncertainty for each parameter is reported in parentheses.

[§§]The subscript "sw'" denotes soil water. Calculated using the equation $\delta^{18}O_c - \delta^{18}O_{water} - T$ relationship for calcite reported in Kim and O'Neil (2). Uncertainty is 0.6% unless otherwise noted in parentheses.

**Table S3. Summary statistics for soil and air temperatures measured at locations relevant to this study**

| Location | Temperature (°C) | | | |
|---|---|---|---|---|
| | Mean | Maximum | Minimum | 1σ |
| Lake Turkana, Kenya (Ileret): 4.28802 N, 36.26055 E, 438 m | | | | |
| August 2008–May 2009 | | | | |
| Veranda shade (air temperature) | 31.3 | 46.2 | 20.1 | 4.3 |
| Site 1, 10 cm depth | 35.6 | 46.1 | 23.6 | 4.0 |
| Site 1, 26 cm depth | 35.4 | 40.1 | 27.8 | 2.2 |
| Site 1, 35 cm depth | 35.3 | 38.9 | 29.1 | 1.9 |
| Site 1, 50 cm depth | 35.2 | 38.2 | 30.1 | 1.6 |
| Gona, Ethiopia: 11.12870 N, 40.45295 E, 619 m December 8–20, 2008 | | | | |
| Mess Tent Shade (air temperature) | 24.7 | 34.2 | 14.8 | 5.1 |
| Acacia Tree Shade (air temperature) | 25.5 | 39.7 | 14.1 | 6.4 |
| Wooded habitat soil, 20 cm depth | 26.4 | 27.8 | 25.0 | 0.6 |
| Wooded habitat soil, 48 cm depth | 28.1 | 28.8 | 27.8 | 0.3 |
| Grassy habitat soil, 10 cm depth | 27.8 | 32.7 | 23.1 | 2.6 |
| Grassy habitat soil, 20 cm depth | 27.4 | 28.8 | 26.0 | 0.7 |
| Grassy habitat soil, 50 cm depth | 28.1 | 28.8 | 27.8 | 0.3 |
| Blackhawk Slide, Lucerne Valley, California: 34.42119 N, 116.789 W, 982 m | | | | |
| May 23–December 12, 2009 | | | | |
| Site 1, 15 cm depth | 25.9 | 40.3 | 2.1 | 8.7 |
| Site 1, 30 cm depth | 25.8 | 34.5 | 7.0 | 6.8 |
| Site 1, 55 cm depth | 25.7 | 31.9 | 11.2 | 5.3 |

1. Ghosh P, et al. (2006) *Geochim Cosmochim Acta* 70:1439.
2. Kim S-T, O'Neil JR (1997) *Geochim Cosmochim Acta* 61:3461.

**Table S4. Summary of stable isotope data for paleosol carbonates from the Turkana Basin, Kenya**

| Sample no. | Member | Burial depth, m[†] | Age, Ma[‡] | *N* | $\delta^{13}C_c$, ‰, PDB[§] | $\delta^{18}O_c$, ‰, PDB[§] | $\Delta_{47}$, ‰, HG[¶] | Temp., °C[††] | $\delta^{18}O_{sw}$, ‰, SMOW[‡‡] |
|---|---|---|---|---|---|---|---|---|---|
| Shungura Formation soil carbonates | | | | | | | | | |
| ET04-OMO-350 | H-2 | 181 | 1.89 | 1 | −7.2 | −1.9 | 0.626 | 29.7 (3.2) | 1.4 |
| ET04-OMO-340 | G-5 | 360 | 2.15 | 1 | −9.6 | −3.1 | 0.612 | 33.0 (3.3) | 0.8 |
| ET04-OMO-335 | G-1 | 389 | 2.2 | 1 | −10.8 | −5.4 | 0.612 | 33.0 (3.3) | −1.5 |
| ET04-OMO-307 | D-2-3 | 504 | 2.45 | 1 | −8.9 | −4.9 | 0.600 | 35.9 (3.4) | −0.4 |
| ET04-OMO-303 | D-1 | 511 | 2.51 | 1 | −7.8 | −4.2 | 0.602 | 35.4 (3.4) | 0.2 |
| ET04-OMO-323 | C-3-5 | 573 | 2.77 | 1 | −9.8 | −4.8 | 0.617 | 32.7 (3.3) | −1.1 |
| ET04-OMO-319 | B-10-2 | 599 | 2.89 | 1 | −8.7 | −3.7 | 0.621 | 30.8 (3.2) | −0.2 |
| Nachukui Formation soil carbonates | | | | | | | | | |
| KN07WT-505 | Nariokotome | 32 | 0.69 | 1 | −6.1 | 2.4 | 0.619 | 31.3 (3.2) | 6.0 |
| KN07WT-502 | Nariokotome | 85 | 1.04 | 2 | −4.7 | 4.1 | 0.597 (0.008) | 36.5 (2.4) | 8.7 (0.4) |
| KN07WT-499 | Nariokotome | 94 | 1.23 | 1 | −7.1 | 0.3 | 0.589 | 38.7 (3.5) | 5.3 |
| KN07WT-492 | Natoo | 169 | 1.42 | 2 | −7.3 | 0.5 | 0.629 (0.007) | 28.8 (2.1) | 3.6 (0.4) |
| KN07WT-488 | Kaitio | 187 | 1.46 | 1 | −6.7 | 0.1 | 0.621 | 30.8 (3.2) | 3.6 |
| KN07WT-513 | Kaitio | 191 | 1.51 | 1 | −6.8 | −4.7 | 0.608 | 33.9 (3.3) | −0.6 |
| KN07WT-521 | Kaitio | 192 | 1.51 | 1 | −7.6 | −2.7 | 0.608 (0.015) | 33.9 (3.8) | 1.4 (0.7) |
| KN07WT-479 | Kaitio | 199 | 1.53 | 1 | −6.3 | −2.7 | 0.626 | 29.6 (3.2) | 0.6 |
| KN07WT-487 | Kaitio | 223 | 1.58 | 1 | −6.0 | 0.4 | 0.606 | 34.4 (3.4) | 4.6 |
| KN07WT-511 | Kalochoro | 396 | 2.04 | 1 | −6.0 | −3.7 | 0.619 | 31.2 (3.2) | −0.1 |
| KN07WT-472 | Kalochoro | 422 | 2.32 | 6 | −9.3 | −3.0 | 0.621 (0.006) | 30.8 (1.8) | 0.5 (0.3) |
| KN07WT-449 | Lomekwi | 533 | 2.93 | 4 | −6.0 | −6.5 | 0.587 (0.005) | 39.2 (1.9) | −1.4 (0.3) |
| KN07WT-444 | Lomekwi | 589 | 3.25 | 2 | −6.8 | −5.7 | 0.611 (0.010) | 33.2 (2.7) | −1.8 (0.5) |
| KN07WT-430 | Lomekwi | 607 | 3.36 | 3 | −4.8 | −3.5 | 0.614 (0.006) | 32.3 (1.9) | 0.3 (0.4) |
| KN07WT-429 | Lomekwi | 618 | 3.42 | 2 | −6.7 | −4.0 | 0.581 (0.005) | 40.8 (1.9) | 1.4 (0.4) |
| KN07WT-437 | Kataboi | 622 | 3.45 | 6 | −8.1 | −5.0 | 0.604 (0.007) | 34.9 (2.2) | −0.7 (0.4) |
| KN07WT-411 | Kataboi | 645 | 3.54 | 1 | −9.2 | −2.4 | 0.614 | 32.4 (3.3) | 1.4 |
| KN07WT-436 | Kataboi | 652 | 3.63 | 1 | −7.8 | −5.3 | 0.633 | 28.0 (3.1) | −2.4 |
| KN07WT-418 | Kataboi | 664 | 3.93 | 2 | −6.7 | −4.1 | 0.611 (0.007) | 33.1 (2.1) | −0.2 (0.4) |
| KN07WT-409 | Lonyumun | 668 | 3.97 | 1 | −8.4 | −3.6 | 0.617 | 31.6 (3.3) | 0.0 |
| Nachukui Formation nonpedogenic carbonates | | | | | | | | | |
| KN07WT-475 | Natoo | 112 | 1.32 | 1 | −5.1 | −2.0 | 0.599 (0.014) | 36.1 (3.8) | 2.5 (0.7) |
| KN07WT-518 | Kaitio | 343 | 1.86 | 1 | −3.6 | −4.4 | 0.599 | 36.1 (3.4) | 0.1 |
| KN07WT-520 | Kalochoro | 347 | 1.87 | 2 | −5.2 | −2.8 | 0.604 (0.009) | 34.9 (2.6) | 1.5 (0.5) |
| KN07WT-482 | Kalochoro | 400 | 2.05 | 1 | −6.3 | −2.9 | 0.619 | 31.3 (3.3) | 0.7 |
| KN07WT-526 | Lomekwi | 463 | 2.53 | 1 | −8.9 | −4.6 | 0.585 | 39.7 (3.5) | 0.6 |
| KN07WT-422 | Lokochot | 647 | 3.57 | 1 | −6.4 | −2.9 | 0.620 | 30.9 (3.2) | 0.6 |

Abbreviations are the same as used and explained in Table S2.

[†]Maximum burial depth, calculated as the cumulative thickness of younger sediments in the same formation, plus the maximum thickness of the overlying Galana Boi Formation.

[‡]Ages are constrained by paleomagnetic reversals and radiometric dates on intercalated volcanic tuffs (1–6). Age uncertainty is ≈0.15–0.05 Ma, as described in *SI Text*.

[§]Replicate extraction level uncertainty in $\delta^{13}C$ and $\delta^{18}O$ is <0.07‰ and 0.06‰, respectively.

[¶]HG, heated gas. Uncertainty in $\Delta_{47}$ is 0.013‰, unless otherwise reported in parentheses.

[††]Calculated using the empirical $\Delta_{47} - T$ relationship of Ghosh et al.(7). Error is reported in parentheses.

[‡‡]Calculated using the $\delta^{18}O_{mineral} - \delta^{18}O_{water} - T$ relationship for calcite reported in Kim and O'Neil (8), where $T$ is based on clumped isotope thermometry. Error is 0.6% unless otherwise noted in parentheses.


1. Kidane T, Otofuji Y-I, Brown FH, Takemoto K, Eshete G (2007) *Earth Planet Sci Lett* 262:240.
2. deMenocal PB, Brown FH (1999) Pliiocene tephra correlations between East African hominid localities, the Gulf of Aden, and the Arabian Sea. *The Evolution of Neogene Terrestrial Ecosystems in Europe*, eds Agusti J, Rook L, Andrews P (Cambridge Univ Press, Cambridge, UK).
3. McDougall I, Brown FH (2008) *J Geol Soc Lond* 165:549.
4. McDougall I, Brown FH (2006) *J Geol Soc Lond* 163:205.
5. Brown FH, Sarna-Wojcicki AM, Meyer CE, Haileab B (1992) *Quat Int* 13/14:55.
6. Feibel CS, Brown FH, McDougall I (1989) Stratigraphic context of fossil hominids from the Omo group deposits: Northern Turkana Basin, Kenya and Ethiopia. *Am J Phys Anthropol* 78: 595–622.
7. Ghosh P, et al. (2006) *Geochim Cosmochim Acta* 70:1439.
8. Kim S-T, O'Neil JR (1997) *Geochim Cosmochim Acta* 61:3461.

**Table S5. $\Delta_{47}$ reproducibility and acid correction factors based on standards analyzed during the course of this study**

| Sample ID | Material | *N* | $\Delta_{47}$ mean 90 °C rxn., ‰ | $\Delta_{47}$ SD, ‰ | $\Delta_{47}$ accepted, 25 °C rxn., ‰ | Acid correction[†], ‰ |
|---|---|---|---|---|---|---|
| 2-8-E | Speleothem | 6 | 0.557 | 0.010 | 0.641[‡] | 0.0842 |
| 95-I-24 | Recrystallized shell | 23 | 0.505 | 0.011 | 0.585[§] | 0.0798 |
| Fast Haga | Chemical precipitate | 53 | 0.547 | 0.013 | — | — |
| NBS-19 | Marble | 17 | 0.275 | 0.019 | 0.352[¶] | 0.0774 |
| UU Carrara | Marble | 15 | 0.276 | 0.009 | — | — |

The "$\Delta_{47}$ mean 90 °C rxn." values correspond to those reported in column J of Table S6 ("$\Delta_{47}$ stretched, v. HG").

[†]The magnitude of this correction is similar to that expected for 90 °C versus 25 °C acid reactions(*31*), but in strict terms this correction compensates for the sum of the differences between this and previous studies, including different reaction temperature, mass spectrometer, and sample extraction system.

[‡]Affek et al. (1).

[§]Huntington et al. (2).

[¶]Ghosh et al. (3).


1. Affek HP, Eiler JM (2006) *Geochim Cosmochim Acta* 70:1.
2. Huntington KW, et al. (2009) Methods and limitations of 'clumped' CO2 isotope (Delta47) analysis by gas-source isotope ratio mass spectrometry. *J Mass Spectrom* 44:1318–1329.
3. Ghosh P, et al. (2006) *Geochim Cosmochim Acta* 70:1439.


## Other Supporting Information Files

Dataset S1 (XLS)